

Anomeric Effects in Sulfonyl Compounds: An Experimental and Computational Study of Fluorosulfonyl Azide, FSO₂N₃, and Trifluoromethylsulfonyl Azide, CF₃SO₂N₃

Xiaoqing Zeng,[†] Michael Gerken,^{*,†,‡} Helmut Beckers,[†] and Helge Willner^{*,†}

Bergische Universität Wuppertal, FB C—Anorganische Chemie, Gauss Strasse 20, D-42097 Wuppertal, Germany, and Department of Chemistry and Biochemistry, The University of Lethbridge, Lethbridge, Alberta T1K 3M4, Canada

Received: April 22, 2010; Revised Manuscript Received: June 9, 2010

Fluorosulfonyl azide, FSO₂N₃, was characterized by IR (gas phase, Ar matrix), and Raman (liquid) spectroscopy. According to the matrix IR spectrum of ¹⁸O-labeled FSO₂N₃, its two oxygen atoms are nonequivalent. This assumption was confirmed by the X-ray crystal structure of FSO₂N₃ at −123 °C, as only one conformer was observed with one of the S=O bonds in synperiplanar position to the N₃ group ($\phi(\text{OS}-\text{NN}) = -14.8(3)^\circ$) with respect to the S–N bond. The same conformation was found for trifluoromethylsulfonyl azide, CF₃SO₂N₃ ($\phi(\text{OS}-\text{NN}) = -23.74(15)^\circ$), in the solid state. The preference of such a synperiplanar configuration between S=O and N₃ was rationalized by a predominant anomeric interaction of $n_\sigma(\text{N}) \rightarrow \sigma^*(\text{S}-\text{O})$, as supported by the experiment and quantum chemical calculations.

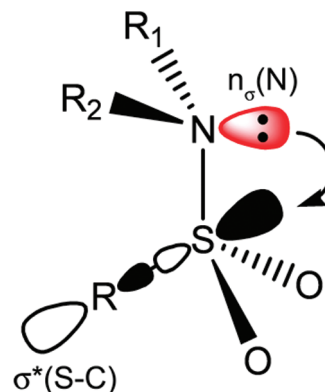
Introduction

Due to the medical and chemical importance, compounds containing sulfur–nitrogen bonds are of long-term interest with a focus on the relationship between structure and reactivity.¹ Of particular interest is the conformation about the sulfur–nitrogen bond in such compounds. Recently, extensive studies have been performed on organic sulfur–nitrogen single-bonded sulfamides (RSO₂NR₂).² These sulfamides were found to adopt an anti-periplanar configuration of the nitrogen lone-pair (n_N) to the S–C bond, and short S–N bonds were always observed, as determined by X-ray crystallography and gas electron diffraction (GED). This conformation was attributed to a dominant anomeric interaction of $n_\sigma(\text{N}) \rightarrow \sigma^*(\text{S}-\text{C})$, which results in partial double-bond character between sulfur and nitrogen (Scheme 1).

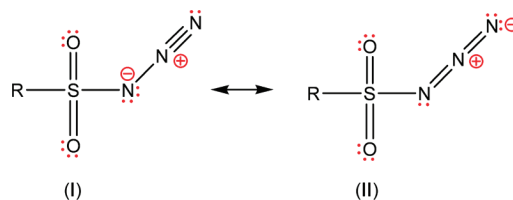
Sulfonyl azides, RSO₂N₃, which have been widely used in organic synthesis,³ should, in principle, also exhibit such $n_\sigma(\text{N}) \rightarrow \sigma^*(\text{S}-\text{C})$ anomeric interactions with a conformation similar to that found for sulfamides due to the availability of lone-pair electrons at the α -nitrogen atom as depicted in Scheme 2. Resonance structure **I** in Scheme 2 is clearly the dominant resonance structure for covalent azides, having two distinctly different lone pairs on the α -nitrogen, i.e., a σ -lone pair and a π -lone pair. Several conformations of sulfonyl azides are possible (Scheme 3), with the sterically favored staggered conformations **c** and **d** and eclipsed conformations **a** and **b** which require electronic (anomeric) effects for their stabilization. Vibrational spectroscopic and GED studies⁴ of trifluoromethylsulfonyl azide, CF₃SO₂N₃, suggested a preference of one single, sterically nonfavorable conformation with a nearly eclipsed orientation of the N₃ group to one S=O bond (conformation **b** in Scheme 3) with a dihedral angle of $\phi(\text{OS}-\text{NN}) = -24(6)^\circ$ derived from GED.^{4a} Similar studies of related molecules, such as CF₃SO₂NCO⁵ and FSO₂NCO,⁶ also revealed conformation **b** in both gas and liquid states.

On the other hand, a GED study suggested the existence of a second conformer **c** for ClSO₂NCO beside conformation **b**.⁷ However, more recent computational and vibrational

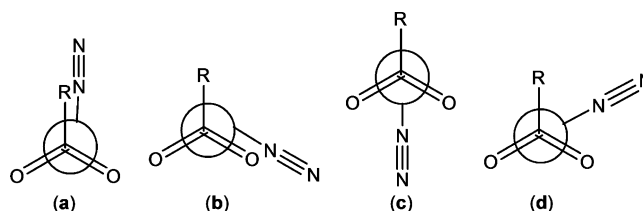
SCHEME 1: Description of $n_\sigma(\text{N}) \rightarrow \sigma^*(\text{S}-\text{C})$ Anomeric Interaction in Sulfamides



SCHEME 2: Resonance Structures of Sulfonyl Azides



SCHEME 3: Possible Conformations of Sulfonyl Azide, RSO₂N₃



* To whom correspondence should be addressed, michael.gerken@uleth.ca and willner@uni-wuppertal.de.

[†] Bergische Universität Wuppertal.

[‡] University of Lethbridge.

studies of the gas, liquid, and solid phases did not find any evidence for the existence of a second conformer beside the dominant conformer **b**.⁸

According to these experimental observations, the stabilizing anomeric interaction, $n_o(N) \rightarrow \sigma^*(S-O)$, seems to be more important in determining the conformation of sulfonyl azides XSO_2N_3 and isocyanates XSO_2NCO than the $n_o(N) \rightarrow \sigma^*(S-C)$ or $\sigma^*(S-X)$ ($X = F, Cl$) interactions. The determination of their high-accuracy molecular structures has not been achieved up to now, partially because these molecules are gaseous or liquid under ambient conditions and, hence, X-ray crystallography is challenging. The possible existence of several conformers (Scheme 3) for sulfonyl azides due to anomeric and steric interactions stimulated us to continue our spectroscopic, structural, and computational studies of simple azides.

As the simplest accessible sulfonyl azide, FSO_2N_3 was first prepared by Ruff in 1965 and has only been characterized by gas-phase IR and UV spectroscopy, as well as mass spectrometry.⁹ A recent computational study of FSO_2N_3 suggested conformer **b** as the only stable conformer.¹⁰ However, no experimental characterization of its structure has been reported. The related compound $CF_3SO_2N_3$ has been widely used as a powerful reagent for preparation of sulfamides and α -nitro- α -diazocarbonyl derivatives.¹¹ Herein we report the unambiguous spectroscopic proof for the nonequivalence of the two oxygen atoms in FSO_2N_3 using matrix-IR spectroscopy of ^{15}N - and ^{18}O -labeled samples, which is further confirmed by determining the molecular structure of FSO_2N_3 using low-temperature X-ray crystallography. This X-ray crystallographic and matrix-IR spectroscopic study is extended to $CF_3SO_2N_3$, confirming the previous prediction of its conformation.⁴ The conformational properties of both compounds were discussed in conjunction with results from quantum chemical calculations.

Experimental Section

Caution! Covalent azides are potentially explosive, although no explosions were experienced during this work, appropriate safety precautions must be taken.

Syntheses of FSO_2N_3 and $CF_3SO_2N_3$. Fluorosulfonyl azide, FSO_2N_3 , was prepared by the reaction of $(FSO_2)_2O$ and NaN_3 according to literature.⁹ For the preparation of ^{15}N -labeled FSO_2N_3 , 1- ^{15}N sodium azide (98 atom % ^{15}N , EURISO-TOP GmbH) was used. For the preparation of ^{18}O -labeled FSO_2N_3 , ^{18}O -labeled $F_2S_2O_5$ was used, which was prepared from the reduction of ^{18}O -labeled $(FSO_3)_2$ (60 atom % ^{18}O)¹² with CO in the gas phase at room temperature. Trifluoromethylsulfonyl azide, $CF_3SO_2N_3$, was prepared by the reaction of $(CF_3SO_2)_2O$ and NaN_3 according to literature.⁹ For the preparation of ^{15}N -labeled $CF_3SO_2N_3$, 1- ^{15}N sodium azide (98 atom % ^{15}N , EURISO-TOP GmbH) was used. The quality of the samples was ascertained by gas-phase IR spectroscopy.

Preparation of the Matrices. Matrix IR spectra were recorded on a FT-IR spectrometer (IFS 66v/S Bruker) in reflectance mode using a transfer optic. A KBr beam splitter and an MCT detector were used in the region of 5000–550 cm^{-1} . A Ge-coated 6 μm Mylar beam splitter combined with a He(I)-cooled Si bolometer and a CsI window at the cryostat were used in the region of 700–180 cm^{-1} . For each spectrum, 200 scans at a resolution of 0.25 cm^{-1} were coadded. The gaseous sample was mixed with argon (1:1000) in a 1-L stainless-steel storage container, and then small amounts (ca. 1 mmol) of the mixture were deposited within 30 min onto the cold matrix support (16 K, Rh-plated Cu block) in high vacuum. Details of the matrix apparatus have been described elsewhere.¹³

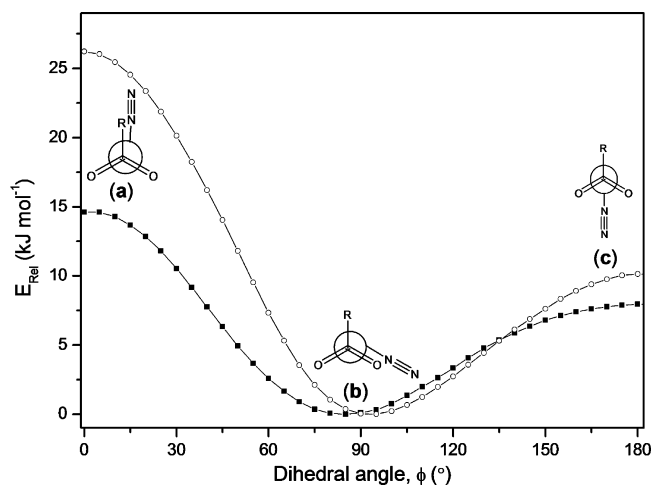


Figure 1. Calculated potential energy curves for internal rotation around the S–N bonds in FSO_2N_3 (■) and $CF_3SO_2N_3$ (○) at the B3LYP/6-311+G(3df) level of theory.

Computational Details. Geometry optimizations were performed using DFT methods (B3LYP,¹⁴ BP86,¹⁵ MPW1PW91¹⁶) with 6-311+G(3df) basis set. Natural bond orbital (NBO) analysis was performed using RHF/6-31G(d) method for the evaluation of donor–acceptor (lone pair–antibonding orbital) interaction energies $E(2)$, based on second-order perturbation theory.¹⁷ The Lewis structure **I** in Scheme 2 was chosen for the NBO analysis by using the NBO \$SCHOOSE keyword in the NBO 5.0 program.¹⁸ The 2-D contour plots of vicinal interactions between preorthogonal natural bond orbitals (PNBOs) are displayed using the program NBOView.¹⁹ All the calculations were performed using the Gaussian 03 software package.²⁰

X-ray Crystal Structure Determination. (a) Crystal Growth and Crystal Mounting. Crystals of FSO_2N_3 and $CF_3SO_2N_3$ were grown in an L-shaped glass tube (0.6 cm o.d., 20 cm length). Small amounts (ca. 20 mg) of the compounds were condensed at -196 °C into the upper part (above the bent) of the tube, which was connected to the vacuum line and subsequently flame-sealed. For the crystallization of FSO_2N_3 and $CF_3SO_2N_3$, the end without sample was immersed into an ethanol cold bath at ca. -80 °C, while the whole setup with cold bath was kept in a refrigerator at -20 °C overnight. The glass tube containing the crystals was cut in a cold nitrogen stream (ca. -70 °C) while maintaining the sample at -196 °C, and the colorless crystals were quickly transferred into a trough cooled by a flow of cold nitrogen and mounted as previously described.²¹ Crystals of FSO_2N_3 and $CF_3SO_2N_3$ having the dimensions $0.290 \times 0.097 \times 0.065$ and $0.123 \times 0.096 \times 0.024$ mm³, respectively, were selected at ca. -70 °C under the microscope.

(b) Collection and Reduction of X-ray Data. Crystals were centered on an Oxford Diffraction Gemini E Ultra diffractometer, equipped with a $2K \times 2K$ EOS CCD area detector, a four-circle kappa goniometer, an Oxford Instruments Cryojet, and sealed-tube Enhanced (Mo) and the Enhanced Ultra (Cu) sources. For the data collection the Mo source emitting graphite-monochromated Mo $K\alpha$ radiation ($\lambda = 0.71073$ Å) was used. The diffractometer was controlled by the CrysAlis^{Pro} graphical user interface (GUI) software.²² Diffraction data collection strategies for FSO_2N_3 and $CF_3SO_2N_3$ were optimized with respect to complete coverage and consisted of four and three ω scans with a width of 1° , respectively. The data collections for FSO_2N_3 and $CF_3SO_2N_3$ were carried out at -123 °C in a 1024×1024 pixel mode using 2×2 pixel binning. Processing of the raw data, scaling of diffraction data, and the application of

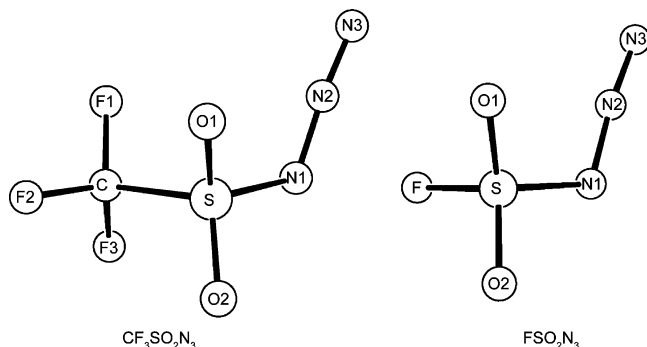


Figure 2. Optimized structure of FSO_2N_3 and $\text{CF}_3\text{SO}_2\text{N}_3$.

TABLE 1: Calculated and Experimental Structural Parameters of FSO_2N_3^a

parameters ^b	B3LYP	BP86	MPW1PW91	X-ray crystallography
$r(\text{S}-\text{O}1)$	1.419	1.434	1.412	1.411(2)
$r(\text{S}-\text{O}2)$	1.411	1.426	1.404	1.404(2)
$r(\text{S}-\text{F})$	1.578	1.603	1.561	1.547(2)
$r(\text{S}-\text{N}1)$	1.672	1.697	1.656	1.648(3)
$r(\text{N}1-\text{N}2)$	1.247	1.252	1.241	1.270(4)
$r(\text{N}2-\text{N}3)$	1.117	1.135	1.113	1.108(4)
$\angle(\text{O}1\text{S}\text{O}2)$	124.4	124.8	124.3	122.82(15)
$\angle(\text{F}\text{S}\text{N}1)$	99.1	98.7	99.2	99.68(14)
$\angle(\text{O}1\text{S}\text{N}1)$	111.4	111.5	111.2	112.76(15)
$\angle(\text{O}2\text{S}\text{N}1)$	106.1	105.5	106.3	106.64(15)
$\angle(\text{S}\text{N}1\text{N}2)$	115.3	115.1	115.1	113.0(2)
$\angle(\text{N}1\text{N}2\text{N}3)$	173.1	172.6	173.5	173.3(3)
$\phi(\text{O}1\text{S}-\text{N}1\text{N}2)$	-28.8	-29.9	-27.8	-14.8(3)
$\phi(\text{O}2\text{S}-\text{N}1\text{N}2)$	-167.0	-168.3	-165.9	-152.4(2)
$\phi(\text{F}\text{S}-\text{N}1\text{N}2)$	82.4	81.4	83.5	97.9(2)
$\phi(\text{S}\text{N}1-\text{N}2\text{N}3)$	176.1	176.0	175.8	168(3)

^a The 6-311+G(3df) basis set was applied for all the calculations.

^b Bond lengths and angles are given in angstroms and degrees, respectively; for labeling of atoms see Figure 2.

an empirical absorption correction were completed by using the CrysAlis^{Pro} program.²²

(c) **Solution and Refinement of the Structure.** The solutions were obtained by direct methods which located the positions

of all atoms. The final refinement was obtained by introducing anisotropic thermal parameters and the recommended weightings for all of the atoms. The maximum electron densities in the final difference Fourier map were located near the heavy atoms. All calculations were performed using the SHELXTL-plus package for the structure determination and solution refinement and for the molecular graphics.²³

Results and Discussion

Quantum Chemical Calculations. In order to locate the minimum on the potential energy surface (PES), energy scans were performed at the B3LYP/6-311+G(3df) level of theory by changing the dihedral angles $\phi(\text{FS}-\text{NN})$ in FSO_2N_3 and $\phi(\text{CS}-\text{NN})$ in $\text{CF}_3\text{SO}_2\text{N}_3$ about the S–N bonds (Figure 1). Surprisingly, only one minimum with the azide group in nearly eclipsed position to one of the S=O bonds was found for both molecules, which corresponds to conformer **b** shown in Scheme 3, while the two C_s symmetric conformers **a** and **c** are transition states on the PES. The energy difference between conformers **b** and **a** is significantly larger for $\text{CF}_3\text{SO}_2\text{N}_3$ (26 kJ mol⁻¹) than that for FSO_2N_3 (14 kJ mol⁻¹), likely as a consequence of the steric repulsion between the CF_3 and N_3 groups. The energy differences between conformers **b** and **c** are very similar for FSO_2N_3 (8 kJ mol⁻¹) and $\text{CF}_3\text{SO}_2\text{N}_3$ (10 kJ mol⁻¹).

The molecular structures for FSO_2N_3 and $\text{CF}_3\text{SO}_2\text{N}_3$ with conformation **b** (Figure 2) were fully optimized with different DFT (B3LYP, BP86, and MPW1PW91) methods, and the obtained structural parameters are listed in Table 1 and Table 2, respectively. Similar structural parameters were obtained for all three DFT methods and the following discussion will only refer to the B3LYP results. The most striking feature for both molecules is the synperiplanar configuration of the N_3 group to one of the S=O bonds in FSO_2N_3 ($\phi(\text{O}1\text{S}-\text{N}1\text{N}2) = -28.8^\circ$) and $\text{CF}_3\text{SO}_2\text{N}_3$ ($\phi(\text{O}1\text{S}-\text{N}1\text{N}2) = -19.3^\circ$), and the synperiplanar S=O bonds for both azides are calculated to be longer than the antiperiplanar ones by 0.008 Å at the B3LYP/6-311+G(3df) level of theory. The CF_3 group in $\text{CF}_3\text{SO}_2\text{N}_3$ was calculated to be staggered with respect to the SO_2N moiety, which is in agreement with steric arguments.

TABLE 2: Calculated and Experimental Structural Parameters of $\text{CF}_3\text{SO}_2\text{N}_3^a$

parameters ^b	B3LYP	BP86	MPW1PW91	GED ^c	X-ray crystallography
$r(\text{S}-\text{O}1)$	1.428	1.443	1.421	1.418(2)	1.4153(13)
$r(\text{S}-\text{O}2)$	1.420	1.436	1.413		1.4085(13)
$r(\text{S}-\text{C})$	1.876	1.899	1.856	1.849(6)	1.832(2)
$r(\text{S}-\text{N}1)$	1.692	1.724	1.673	1.668(4)	1.6482(15)
$r(\text{F}1-\text{C})$	1.331	1.342	1.323	1.321(3)	1.319(2)
$r(\text{F}2-\text{C})$	1.324	1.336	1.316		1.316(2)
$r(\text{F}3-\text{C})$	1.323	1.334	1.315		1.313(2)
$r(\text{N}1-\text{N}2)$	1.246	1.250	1.240	1.252(7)	1.276(2)
$r(\text{N}2-\text{N}3)$	1.117	1.136	1.113	1.120(6)	1.106(2)
$\angle(\text{O}1\text{S}\text{O}2)$	123.9	124.3	123.9		123.02(9)
$\angle(\text{O}1\text{S}\text{N}1)$	110.6	110.7	110.5	111.1(22)	112.39(7)
$\angle(\text{O}2\text{S}\text{N}1)$	106.0	105.3	106.1	106.9(22)	105.80(8)
$\angle(\text{C}\text{S}\text{N}1)$	99.8	99.4	99.82	107.5(11)	101.33(9)
$\angle(\text{S}\text{N}1\text{N}2)$	115.3	114.8	115.0	111.6(15)	111.99(12)
$\angle(\text{N}1\text{N}2\text{N}3)$	173.6	173.3	173.9	173.1(35)	173.52(18)
$\phi(\text{O}1\text{S}-\text{N}1\text{N}2)$	-19.3	-19.1	-19.5	-24(6)	-23.74(15)
$\phi(\text{O}2\text{S}-\text{N}1\text{N}2)$	-156.1	-156.0	-156.4		-160.54(12)
$\phi(\text{C}\text{S}-\text{N}1\text{N}2)$	92.8	93.1	92.5	89(6)	88.49(14)
$\phi(\text{S}\text{N}1-\text{N}2\text{N}3)$	172.2	172.6	172.4		176.2(16)

^a The 6-311+G(3df) basis set was applied for all the calculations. ^b Bond lengths and angles are given in angstroms and degrees, respectively; for labeling of atoms see Figure 2. ^c Reference.^{4a}

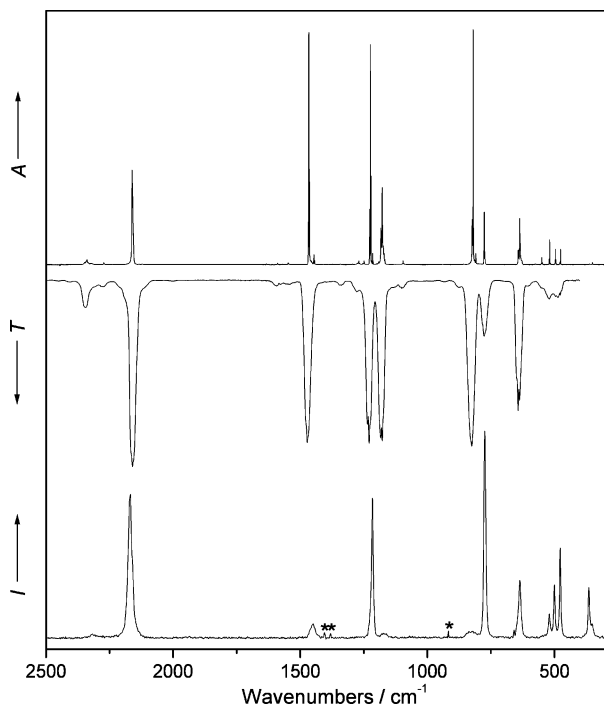


Figure 3. Upper trace: IR spectrum of FSO_2N_3 isolated in an Ar-matrix at 16 K (absorbance A , resolution 0.25 cm^{-1}). Middle trace: IR spectrum of gaseous FSO_2N_3 at 300 K (transmission T , resolution 2 cm^{-1}). Lower trace: Raman spectrum of liquid FSO_2N_3 at 300 K (Raman intensity I , resolution 2 cm^{-1}). Bands associated with impurity of CH_3NO_2 are marked with an asterisk.

Vibrational Spectroscopy. The Ar-matrix IR, gas-phase IR, and liquid-state Raman spectra were recorded of FSO_2N_3 and are shown in Figure 3. The experimental frequencies are listed in Table 3 together with the vibrational frequencies obtained from B3LYP/6-311+G(3df) calculations and their corresponding assignments.

The N_3 and SO_2 asymmetric stretches appeared at 2162.3 and 1466.2 cm^{-1} in the Ar-matrix IR spectrum, respectively, which are in good agreement with the corresponding calculations of 2287 and 1474 cm^{-1} by B3LYP/6-311+G(3df). In contrast to the experimental observations, the order of the symmetric stretches of these two groups was interchanged by all three DFT methods (B3LYP, BP86, MPW1PW91), e.g., the B3LYP/6-311+G(3df) calculations (Table 3) predicted a higher frequency for sym. N_3 stretch at 1256 cm^{-1} than sym. SO_2 stretch at 1230

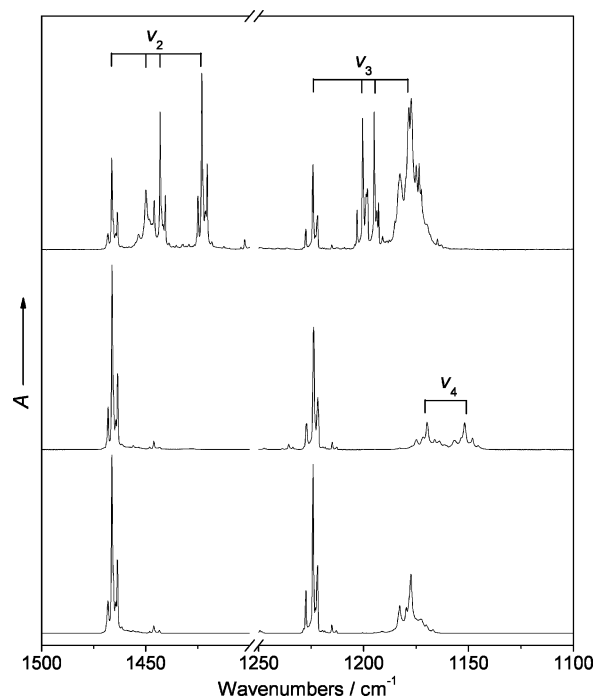


Figure 4. Matrix-IR spectra of FSO_2N_3 (absorbance A , resolution 0.25 cm^{-1}) in the range of $1500\text{--}1100\text{ cm}^{-1}$. Lower trace: FSO_2N_3 ; Middle: 1:1 mixture of $\text{FSO}_2^{13}\text{NNN}$ and $\text{FSO}_2\text{NN}^{13}\text{N}$; Upper: 1:2.7:1.9 mixture of FSO_2N_3 , $\text{FS}^{16}\text{O}(\text{}^{18}\text{O})\text{N}_3$, and $\text{FS}^{18}\text{O}_2\text{N}_3$.

cm^{-1} . The correct assignment of the experimental bands at 1224.1 and 1177.4 cm^{-1} to the respective sym. stretches of N_3 and SO_2 was confirmed by their $^{16/18}\text{O}$ and $^{14/15}\text{N}$ isotopic shifts (Figure 4).

Most of the bands in the matrix IR spectrum are flanked by bands attributable to different matrix sites with frequency differences within a few wavenumbers ($<5\text{ cm}^{-1}$); no evidence for the existence of a second conformer could be obtained. The gas-phase IR and liquid-phase Raman spectra also show no additional bands that correspond to a second conformer. Therefore, in accordance with the computational results, only one conformer is present in the gas and liquid states, as well as in the Ar matrix.

According to the calculations, the two $\text{S}=\text{O}$ bonds are different by 0.008 \AA for all three DFT methods (Table 1). Thus, for the mixed-labeled $^{18}\text{O}\text{S}^{16}\text{O}$ moiety two different frequencies are expected for several fundamental vibrations in the matrix

TABLE 3: Experimental and Calculated Vibrational Frequencies (cm^{-1}) of FSO_2N_3

IR (gas-phase)	experimental ^a		calculated ^c	mode/assignment
	IR (Ar-matrix) ^b	Raman (liquid)		
2161 vs	2162.3 s	2168 s	2287 (393)	ν_1 , N_3 asym. stretch
1473 s	1466.2 vs	1450 w	1474 (234)	ν_2 , SO_2 asym. stretch
1230 s	1224.1 vs	1216 s	1230 (174)	ν_3 , SO_2 sym. stretch
1181 s	1177.4 s	1171 vw	1256 (274)	ν_4 , N_3 sym. stretch
826 s	819.1 vs	824 vw	790 (247)	ν_5 , $\text{S}-\text{F}$ stretch
777 m	775.4 m	774 vs	752 (59)	ν_6 , $\text{S}-\text{N}$ stretch
640 s	635.9 s	636 s	638 (152)	ν_7 , in-plane N_3 deformation
520 w, br	549.3 m	520 m	581 (6)	ν_8 , out-of-plane N_3 deformation
	518.2 m	500 m	508 (14)	ν_9 , SO_2 bending
485 w, sh	496.0 m	478 s	484 (10)	ν_{10} , FSO bending
	475.6 m		472 (6)	ν_{11}
	350.2 w	364 m	353 (3)	ν_{12}

^a Experimental band positions and intensities: vs, very strong; s, strong; m, medium strong; w, weak; vw, very weak; sh, shoulder; br, broad.

^b Most intensive matrix site. ^c Calculated IR data at the B3LYP/6-311+G(3df) level with intensities (km mol^{-1}) in parentheses. The remaining last three fundamental vibrations are at 340 (1), 157 (1), 60 (<1) cm^{-1} .

TABLE 4: Experimental^a and Calculated^b ^{16/18}O Isotopic Shifts (cm⁻¹) for FSO₂N₃

	$\Delta\nu(^{16/18}\text{O}1)^c$		$\Delta\nu(^{16/18}\text{O}2)^d$		$\Delta\nu(^{16/18}\text{O}1^{16/18}\text{O}2)^e$	
	exptl	calcd	exptl	calcd	exptl	calcd
ν_1	0.2	0.0	0.2	0.0	0.2	0.0
ν_2	16.4	16.3	23.1	23.4	43.1	44.1
ν_3	29.2	30.9	23.6	25.0	50.5	51.5
ν_4	0.0	0.0	0.0	0.1	0.0	0.1
ν_5	0.0	0.3	1.1	0.9	1.6	1.3
ν_6	3.7	3.2	1.5	1.2	5.2	4.5
ν_7	3.9	3.7	5.3	4.8	9.6	8.5
ν_8	0.0	0.0	0.0	0.0	0.0	0.0
ν_9	7.1	6.9	7.1	7.1	15.3	15.1
ν_{10}	5.9	5.9	7.9	7.4	13.2	12.5
ν_{11}	4.7	4.9	3.0	3.3	7.8	8.4
ν_{12}	2.9	2.8	2.2	2.2	5.2	5.1

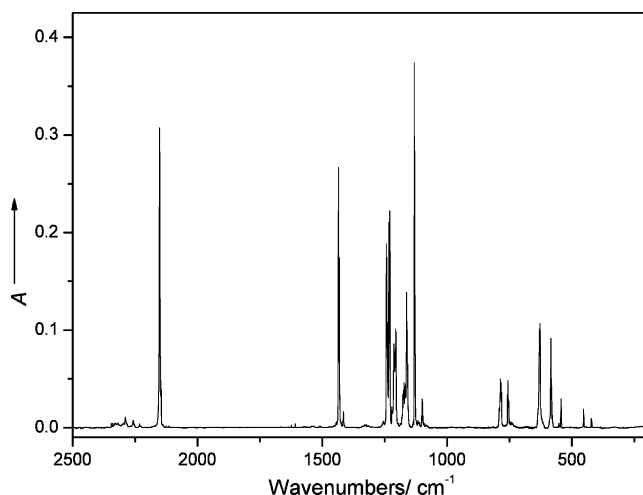
^a Observations in Ar matrix. ^b Calculations at the B3LYP/6-311+G(3df) level of theory. ^c ¹⁸O isotopic labeling of O1 (Figure 2). ^d ¹⁸O isotopic labeling of O2 (Figure 2). ^e ¹⁸O isotopic labeling of both O1 and O2 (Figure 2).

IR spectrum of FSO₂N₃. The IR spectra of Ar-matrix isolated FSO₂N₃:FS(¹⁶O)(¹⁸O)N₃:FS¹⁸O₂N₃ = 1:2.7:1.9 in the range of 1500–1100 cm⁻¹ are shown in Figure 4 (upper trace). For comparison, the IR spectrum of ¹⁵N-labeled FSO₂N₃ (FSO₂¹⁵NNN:FSO₂NN¹⁵N = 1:1) is also shown (Figure 4, middle trace), and the ^{14/15}N isotopic shifts are given in Table S1 (Supporting Information). The experimental ^{16/18}O isotopic shifts are listed in Table 4, which show very good agreement with the calculated values. Significant differences between the experimental and predicted ^{14/15}N isotopic shifts were observed for ν_1 (experimental, 5.5 cm⁻¹; calculated, 1.2 cm⁻¹) and ν_{11} (experimental, 1.6 cm⁻¹; calculated, 3.1 cm⁻¹), suggesting strong anharmonic perturbations.

As is shown in Figure 4 (upper trace), the mono-¹⁸O-labeling of the two oxygen atoms, O1 and O2 in Figure 2, lead to different isotopic shifts for the vibrational modes of ν_2 (asym. SO₂ stretch) and ν_3 (sym. SO₂ stretch). For the asymmetric stretch, ¹⁸O-labeling of O1 causes a shift of 16.4 cm⁻¹, which is significantly smaller than the effect of ¹⁸O-labeling of O2 (23.1 cm⁻¹). The corresponding isotopic bands for ν_2 show different line shapes, probably due to vibrational coupling. Well-separated bands were observed for the sym. SO₂ stretch with experimental ^{16/18}O isotopic shifts of 29.2 and 23.6 cm⁻¹. A similar isotopic splitting pattern was also observed for the FSO bending mode (ν_{10}) in the region of 530–460 cm⁻¹ (Figure S1 in Supporting Information), but for the SO₂ bending mode (ν_9), only three bands appeared, indicating very close ^{16/18}O isotopic shifts (7.1 cm⁻¹) for FS(¹⁶O1)(¹⁸O2)N₃ and FS(¹⁸O1)(¹⁶O2)N₃, which is consistent with the calculated isotopic shifts of 7.1 and 6.9 cm⁻¹ for these two isotopomers, respectively.

The IR spectrum of Ar-matrix isolated CF₃SO₂N₃ is shown in Figure 5, the observed IR frequencies are listed in Table 5 and compared with the gas-phase and calculated IR spectra. In agreement with the previous IR (gas-phase) and Raman (liquid) studies,^{4b} the assignments of all observed vibrational bands (gas-phase, liquid, and Ar-matrix) can be assigned in terms of a single conformer.

The assignments of the Ar-matrix IR spectrum were aided by ¹⁵N labeling experiments (Table S2 in Supporting Information), but the vibrations are perturbed by anharmonic resonances as suggested by the large differences between the observed and calculated isotopic shifts for the vibrations involving the N₃ and SO₂ moieties in CF₃SO₂¹⁵NNN, i.e., ν_1 , ν_4 , ν_6 . The S–N stretch

**Figure 5.** IR spectrum of Ar-matrix isolated CF₃SO₂N₃ at 16 K (absorbance A, resolution 0.25 cm⁻¹).**TABLE 5: Experimental and Calculated IR Frequencies (cm⁻¹) of CF₃SO₂N₃**

experimental ^a		calculated ^c	mode/assignment	
IR (gas phase)	IR (Ar matrix) ^b			
2152 s	2151.6 s	2280 (444)	ν_1 , N ₃ asym. stretch	
1440 s	1434.6 s	1438 (216)	ν_2 , SO ₂ asym. stretch	
1237 s	1242.5 s	1255 (188)	ν_3 , CF ₃ asym. stretch	
1220 s, sh	1231.7 s	1229 (366)	ν_4 , SO ₂ sym. stretch	
	1208.7 m	1213 (193)	ν_5 , CF ₃ asym. stretch	
1168 s	1162.3 m	1191 (51)	ν_6 , N ₃ sym. stretch	
1133 s	1130.7 vs	1114 (261)	ν_7 , CF ₃ sym. stretch	
784 m	786.6 m	770 (28)	ν_8 , CF ₃ deformation	
755 m	756.6 m	737 (64)	ν_9 , S–N stretch	
632 s	628.5 m	630 (197)	ν_{10} , N ₃ in-plane deformation	
		579 (1)	ν_{11} , N ₃ out-of-plane deformation	
		577 (80)	ν_{12} , SO ₂ deformation	
		551 (<1)	ν_{13} , CF ₃ deformation	
546 w	544.7 m	536 (14)	ν_{14} , CF ₃ deformation	
452 w	453.4 m	443 (2)	ν_{15}	
421 w	422.6 w	418 (4)	ν_{16}	
		318 (0)	ν_{17}	
		315 (0)	ν_{18}	
	207.1 vw	279 (1)	ν_{19}	
	203.9 vw	195 (2)	ν_{20}	
		190.0 vw	179 (3)	ν_{21}

^a Experimental band positions and intensities: vs, very strong; s, strong; m, medium strong; w, weak; vw, very weak; sh, shoulder; br, broad. ^b Most intensive matrix site. ^c Calculated IR data at the B3LYP/6-311+G(3df) level with intensities (km mol⁻¹) in parentheses.

(ν_9) for CF₃SO₂N₃ appeared at 756.6 cm⁻¹ and it is lower than that of FSO₂N₃ at 775.4 cm⁻¹ in Ar matrix, indicating a slightly stronger and shorter S–N bond in the latter molecule.

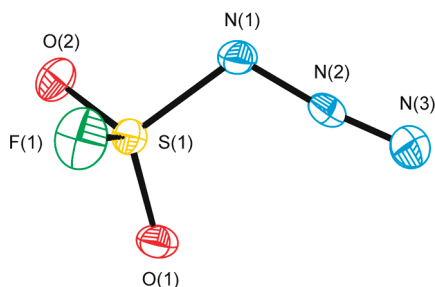
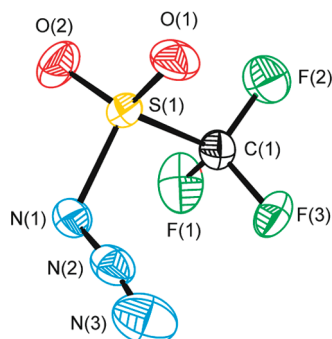
X-ray Crystallography. The two title azides, FSO₂N₃ and CF₃SO₂N₃, are liquid at room temperature; crystals suitable for single-crystal X-ray crystallography were grown by slow evaporation at –20 °C and condensation at –80 °C in an evacuated L-shaped flame-sealed glass tube. The crystallographic data for both compounds are listed in Table 6.

Fluorosulfonyl azide, FSO₂N₃, crystallizes in the monoclinic *Cc* space group, with four molecules in the unit cell. The molecular structure of the FSO₂N₃ molecule is shown in Figure 6, and the structural parameters are given in Table 1. The *C*₁ symmetric molecule contains two nonequivalent oxygen atoms, the S1=O1 bond shows a nearly eclipsed conformation (synperiplanar) to the N1–N2 bond with a torsion angle of –14.8(3)° ($\phi(\text{O}1\text{S}1-\text{N}1\text{N}2)$), while the S1=O2 bond exhibits an antiperiplanar conformation to the N1–N2 bond ($\phi(\text{O}2\text{S}1-\text{N}1\text{N}2) = -152.4(2)^\circ$). In agreement

TABLE 6: Crystallographic Data of FSO₂N₃ and CF₃SO₂N₃

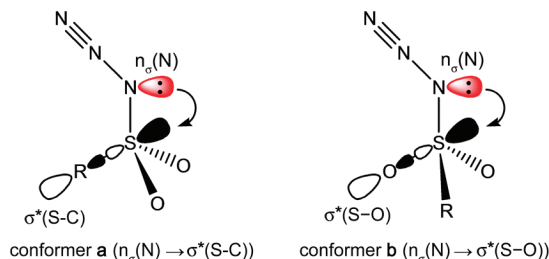
chemical formula	FN ₃ O ₂ S	CF ₃ N ₃ O ₂ S
space group	Cc	P2 ₁ /c
<i>a</i> (Å)	7.0017(13)	5.0666(4)
<i>b</i> (Å)	13.5124(15)	17.0136(10)
<i>c</i> (Å)	5.0170(9)	7.0041(5)
α (deg)	90	90
β (deg)	121.37(3)	106.130(7)
γ (deg)	90	90
<i>V</i> (Å ³)	405.25(12)	579.99(7)
<i>Z</i> (molecules/unit cell)	4	4
mol wt	125.09	175.10
calcd density (g cm ⁻³)	2.050	2.005
<i>T</i> (°C)	-123	-123
μ (mm ⁻¹)	0.698	0.567
<i>R</i> ₁ ^a	0.0260	0.0316
w <i>R</i> ₂ ^b	0.0649	0.0673

^a *R*₁ is defined as $\sum |F_o| - |F_c| / \sum |F_o|$ for $I > 2\sigma(I)$. ^b w*R*₂ is defined as $[\sum w(F_o^2 - F_c^2)^2 / \sum w(F_o^2)]^{1/2}$ for $I > 2\sigma(I)$.

**Figure 6.** View of the FSO₂N₃ molecule in the unit cell. Thermal ellipsoids are drawn at the 50% probability level.**Figure 7.** View of the CF₃SO₂N₃ molecule; thermal ellipsoids are drawn at the 50% probability level.

with the optimized gas-phase geometry, the synperiplanar S=O bond (1.411(2) Å) is significantly longer than that of the anti-periplanar one (1.404(2) Å). The S–F bond length is 1.547(2) Å and longer than those of F₂SO₂ (1.514(2) Å)²⁴ and FSO₂Cl (1.5377(12) Å)²⁴ in the solid state, consistent with the relative electronegativity of the ligands N₃ < Cl < F. These solid-state structural features are generally reproduced by the DFT calculations for the gas phase, and no significant through-space nonbonded interactions were observed in the solid.

Trifluoromethylsulfonyl azide, CF₃SO₂N₃, crystallizes in the monoclinic *P*2₁/*c* space group, with four molecules in the unit cell. The molecular structure is shown in Figure 7, the structural parameters are listed in Table 2 and compared with the GED results. The structural parameters of CF₃SO₂N₃ in the solid state are in overall excellent agreement with those obtained by GED in the gas phase,^{4a} but with much higher accuracy. The S1=O1 and S1=O2 bonds are synperiplanar and antiperiplanar to the azide group with dihedral angle of $\phi(\text{O1S1} - \text{N1N2}) = -23.74(15)^\circ$ and $\phi(\text{O2S1} - \text{N1N2}) = -160.54(12)^\circ$, respec-

SCHEME 4: Description of Possible Anomeric Interactions in Sulfonyl Azides RSO₂N₃

tively, and the former S=O bond (1.4153(13) Å) is longer than the latter (1.4085(13) Å). The S1–N1 bond length in CF₃SO₂N₃ is 1.6482(15) Å, which is very close to that in FSO₂N₃ (1.648(3) Å). The angle ($\angle(\text{SN1N2})$) at the bridging nitrogen atom (N1) is 111.99(12)°, and it is slightly smaller than that in FSO₂N₃ (113.0(2)°). The CF₃ group is staggered to the SO₂N moiety along the C–S bond. The crystal packing of CF₃SO₂N₃ is shown in Figure S3 (Supporting Information); clearly the molecules are aligned to have minimum dipole moment for the solid.

Conformational Properties. Recently, Besenyei et al.²⁵ reported the crystal structure of six arenesulfonyl azides and found that the N₃ group exhibits a synperiplanar conformation to one of the S=O double bonds, while the other one is in an antiperiplanar position. The S=O bond lengths are strongly perturbed by through-space nonbonded interactions, thus no conclusive information could be obtained for the subtle intramolecular electronic interactions. In order to rule out any intermolecular effects on the conformation, the IR spectrum of matrix isolated FSO₂N₃ combined with ¹⁸O-labeling was recorded, which clearly showed the structural non-equivalence of the two oxygen atoms in the molecule, ruling out through-space nonbonded interactions as the cause for this conformation. In addition, the agreement between the gas-phase and the solid-state structures of CF₃SO₂N₃ indicates the negligible effects of packing on the conformation. As a consequence, it can be assumed that electronic (anomeric) effects are dominant in determining the conformation and that the crystal structure of FSO₂N₃ is also a good model for the gas-phase structure. These assumptions are supported by the computational results (vide supra).

The theoretically predicted and also experimentally determined structures of FSO₂N₃ and related CF₃SO₂N₃ revealed a synperiplanar configuration of the longer S=O bond to the N₃ group, while the shorter S=O bond is in an antiperiplanar configuration. All of these structural features can be viewed as a function of the anomeric interaction of $n_o(\text{N}) \rightarrow \sigma^*(\text{S}-\text{O})$, i.e., the donation of electron density of the σ -type lone-pair on the α -nitrogen $n_o(\text{N})$ into the antibonding orbital of the synperiplanar (with respect to the N₃ group) S=O bond, $\sigma^*(\text{S}-\text{O})$. As an additional result, larger angles of $\angle\text{O1SN1}$ are observed for both molecules by X-ray crystallography (FSO₂N₃ 112.76(15)°, CF₃SO₂N₃ 112.39(7)°) than $\angle\text{O2SN1}$ (FSO₂N₃ 106.64(15)°, CF₃SO₂N₃ 105.80(8)°).

In principle as shown in Scheme 4, two competing anomeric interactions $n_o(\text{N}) \rightarrow \sigma^*(\text{S}-\text{F})$ and $n_o(\text{N}) \rightarrow \sigma^*(\text{S}-\text{O})$ in FSO₂N₃, and $n_o(\text{N}) \rightarrow \sigma^*(\text{S}-\text{C})$ and $n_o(\text{N}) \rightarrow \sigma^*(\text{S}-\text{O})$ in CF₃SO₂N₃ are expected to determine the conformation of these molecules. According to the RHF/6-31G(d) calculations, the energies for the acceptor orbitals of $\sigma^*(\text{S}-\text{F})$ (0.181 au) and $\sigma^*(\text{S}-\text{C})$ (0.243 au) are much higher than the other acceptor orbital $\sigma^*(\text{S}-\text{O})$ in FSO₂N₃ (0.111 au) and CF₃SO₂N₃ (0.116 au), respectively, which renders the donation of σ -type nitrogen lone pair, $n_o(\text{N})$, to $\sigma^*_{\text{S}-\text{O}}$ more favorable.

The overlap between preorthogonal natural bond orbitals (PN-BOs) reflects the strength of the associated NBO Fock matrix

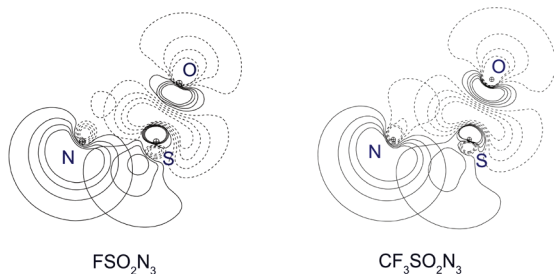


Figure 8. Contour plots of the vicinal $n_o(N) \rightarrow \sigma^*(S-O)$ interactions in FSO_2N_3 and $CF_3SO_2N_3$ using RHF/6-31G(d) calculated preorthogonal natural bond orbitals (PNBOs). Projections on the plane are defined by the atoms shown in the plots.

elements (F_{ij}), as shown in Figure 8. The “in-plane” nitrogen lone pair, denoted as $n_o(N)$, is found to strongly interact with the antibonding orbital of the $S=O$ bond that is antiperiplanar with respect to the nitrogen lone pair. The NBO analysis of the predominant resonance structure **I** (Scheme 2) yields interaction energies based on second-order perturbation theory, $E(2)$, and NBO occupancies of antibonding orbitals, which are listed in Table S3 (Supporting Information). The $n_o(N) \rightarrow \sigma^*(S-O)$ interaction energies $E(2)$ were calculated (RHF/6-31G(d)) to be 67.3 and 59.9 kJ mol^{-1} for FSO_2N_3 and $CF_3SO_2N_3$, respectively. These large interaction energies are also reflected in the significant NBO occupancies for the $\sigma^*(S-O)_{\text{syn}}$ antibonding orbitals of 0.27 and 0.20 for FSO_2N_3 and $CF_3SO_2N_3$, respectively.

Conclusions

Vibrational spectroscopic studies of FSO_2N_3 in gas phase, Ar matrix, and liquid state suggest the existence of only one conformer, and the two oxygen atoms were supposed to be structurally nonequivalent based on the matrix IR spectrum of mixed ^{18}O -labeled FSO_2N_3 . These spectroscopic results were confirmed by its structure determined by X-ray crystallography, which shows that the azide group is synperiplanar to one $S=O$ group ($\phi(\text{OIS-NIN2}) = -14.8(3)^\circ$) and antiperiplanar to the other one ($\phi(\text{O2S-NIN2}) = -152.4(2)^\circ$) with small but significant differences in $S=O$ bond lengths. Similar conformational and structural properties were also observed for $CF_3SO_2N_3$ in both gas phase (GED) and solid state (X-ray crystallography). The exclusive presence of the same sterically unfavorable conformation for FSO_2N_3 and $CF_3SO_2N_3$ in all states is a consequence of the electronic, anomeric $n_o(N) \rightarrow \sigma^*(S-O)$ interaction, as confirmed by DFT calculations. This anomeric effects also explain the longer synperiplanar $S=O$ bond than the antiperiplanar $S=O$ bond in both sulfonyl azides.

Acknowledgment. X. Z. expresses his thanks to the Alexander von Humboldt Foundation for a research grant; H. B. and H. W. acknowledge support from the Deutsche Forschungsgemeinschaft and the Fonds der Chemischen Industrie and M.G. acknowledges the University of Lethbridge for granting a study leave. We are grateful to Dr. Wenda for providing $(CF_3SO_2)_2O$.

Supporting Information Available: Matrix-IR spectra (Figure S1) of FSO_2N_3 in the range of $530\text{--}460\text{ cm}^{-1}$; packing diagrams of FSO_2N_3 (Figure S2) and $CF_3SO_2N_3$ (Figure S3) in the solid state; experimental and calculated $^{14/15}\text{N}$ isotopic shifts of FSO_2N_3 (Table S1) and $CF_3SO_2N_3$ (Table S2); NBO second-order perturbative estimates of interaction energies and NBO occupancies (Table S3); X-ray crystallographic files in CIF format for the structure determinations of FSO_2N_3 and

$CF_3SO_2N_3$. This material is available free of charge via the Internet at <http://pubs.acs.org>.

References and Notes

- (1) See for examples: (a) Claus, P. K. In *The Chemistry of Sulphenic Acids and Their Derivatives*; Patai, S., Ed.; John Wiley & Sons: New York, 1990; Chapter 17. (b) Davis, F. A. *J. Org. Chem.* **2006**, *71*, 8993–9003. (c) Davis, F. A.; Kluger, E. W. *J. Am. Chem. Soc.* **1976**, *98*, 302–303.
- (2) See for examples: (a) Modarresi-Alam, A. R.; Amirazizi, H. A.; Bagheri, H.; Bijanzadeh, H.-R.; Kleinpeter, E. *J. Org. Chem.* **2009**, *74*, 4740–4746. (b) Denehy, E.; White, J. M.; Williams, S. J. *Chem. Commun.* **2006**, 314–316. (c) Petrov, V.; Petrova, V.; Girichev, G. V.; Oberhammer, H.; Giricheva, N. I.; Ivanov, S. *J. Org. Chem.* **2006**, *71*, 2952–2956. (d) Wang, L. J.; Mezey, P. G. *J. Phys. Chem. A* **2005**, *109*, 8819–8825.
- (3) See for examples: (a) Panchaud, P.; Chabaud, L.; Landais, Y.; Ollivier, C.; Renaud, P.; Zigmantas, S. *Chem.-Eur. J.* **2009**, *10*, 3606–3614. (b) Panchaud, P.; Chabaud, L.; Landais, Y.; Ollivier, C.; Renaud, P.; Zigmantas, S. *Chem.-Eur. J.* **2004**, *10*, 3606–3614. (c) Rauschel, J.; Pitram, S. M.; Fokin, V. V. *Org. Lett.* **2008**, *10*, 3385–3388.
- (4) (a) Haist, R.; Mack, H.-G.; Della Védova, C. O.; Cutín, E. H.; Oberhammer, H. *J. Mol. Struct.* **1998**, *445*, 197–205. (b) Álvarez, R. M. S.; Cutín, E. H.; Romano, R. M.; Mack, H.-G.; Della Védova, C. O. *Spectrochim. Acta, Part A* **1998**, *54*, 605–615.
- (5) Álvarez, R. M. S.; Cutín, E. H.; Mack, H.-G.; Della Védova, C. O. *J. Raman Spectrosc.* **1998**, *28*, 277–281.
- (6) (a) Della Védova, C. O.; Cutín, E. H.; Mack, H.-G.; Oberhammer, H. *J. Mol. Struct.* **1996**, *380*, 167–170. (b) Álvarez, R. M. S.; Cutín, E. H.; Mack, H.-G.; Della Védova, C. O. *J. Mol. Struct.* **1994**, *323*, 29–38.
- (7) Brunvoll, J.; Hargittai, I.; Seip, R. *J. Chem. Soc., Dalton Trans.* **1978**, 299–302.
- (8) (a) Durig, J. R.; Zhou, L.; Gounev, T. K.; Guirgis, G. A. *Spectrochim. Acta, Part A* **1997**, *53*, 1581–1593. (b) Álvarez, R. M. S.; Cutín, E. H.; Della Védova, C. O. *Spectrochim. Acta, Part A* **1995**, *51*, 555–561. (c) Jo, O. L.; Graybeal, J. D.; Lovas, F. J.; Suenram, R. D. *J. Mol. Spectrosc.* **1992**, *152*, 261–273.
- (9) Ruff, J. K. *Inorg. Chem.* **1965**, *4*, 567–570.
- (10) Badawi, H. M.; Förner, W.; Al-Ghamdi, K. S. *J. Mol. Struct. (THEOCHEM)* **2003**, *624*, 225–232.
- (11) (a) Charette, A. B.; Wurz, R. P.; Ollevier, T. *J. Org. Chem.* **2000**, *65*, 9252–9254. (b) Wurz, R. P.; Lin, W.; Charette, A. B. *Tetrahedron Lett.* **2003**, *44*, 8845–8848. (c) Benati, L.; Nanni, D.; Spagnolo, P. *J. Org. Chem.* **1999**, *64*, 5132–5138.
- (12) Zhang, D.; Wang, C.; Mistry, F.; Powell, B.; Aubke, F. *J. Fluorine Chem.* **1996**, *76*, 83–89.
- (13) Schnöckel, H. G.; Willner, H. In *Infrared and Raman Spectroscopy, Methods and Applications*; Schrader, B., Ed.; VCH: Weinheim, 1994.
- (14) Becke, A. D. *J. Chem. Phys.* **1993**, *98*, 5648–5652.
- (15) Perdew, J. P. *Phys. Rev. B* **1986**, *33*, 8822–8824.
- (16) Adamo, C.; Barone, V. *J. Chem. Phys.* **1998**, *108*, 664–675.
- (17) Reed, A. E.; Curtiss, L. A.; Weinhold, F. *Chem. Rev.* **1988**, *88*, 899–926.
- (18) Weinhold, F., Ed.; *NBO 5.0 Program Manual*; Theoretical Chemistry Institute, University of Wisconsin: Madison, WI, 2001.
- (19) Wendt, M.; Weinhold, F.; *NBOView 1.1: NBO Orbital Graphics*; University of Wisconsin: Madison, 2001.
- (20) Frisch, M. J.; Trucks, G. W.; Schlegel, H. B.; Scuseria, G. E.; Robb, M. A.; Cheeseman, J. R.; Montgomery, J. A., Jr.; Vreven, T.; Kudin, K. N.; Burant, J. C.; Millam, J. M.; Iyengar, S. S.; Tomasi, J.; Barone, V.; Mennucci, B.; Cossi, M.; Scalmani, G.; Rega, N.; Petersson, G. A.; Nakatsuji, H.; Hada, M.; Ehara, M.; Toyota, K.; Fukuda, R.; Hasegawa, J.; Ishida, M.; Nakajima, T.; Honda, Y.; Kitao, O.; Nakai, H.; Klene, M.; Li, X.; Knox, J. E.; Hratchian, H. P.; Cross, J. B.; Adamo, C.; Jaramillo, J.; Gomperts, R.; Stratmann, R. E.; Yazyev, O.; Austin, A. J.; Cammi, R.; Pomelli, C.; Ochterski, J. W.; Ayala, P. Y.; Morokuma, K.; Voth, G. A.; Salvador, P.; Dannenberg, J. J.; Zakrzewski, V. G.; Dapprich, S.; Daniels, A. D.; Strain, M. C.; Farkas, O.; Malick, D. K.; Rabuck, A. D.; Raghavachari, K.; Foresman, J. B.; Ortiz, J. V.; Cui, Q.; Baboul, A. G.; Clifford, S.; Cioslowski, J.; Stefanov, B. B.; Liu, G.; Liashenko, A.; Piskorz, P.; Komaromi, I.; Martin, R. L.; Fox, D. J.; Keith, T.; Al-Laham, M. A.; Peng, C. Y.; Nanayakkara, A.; Challacombe, M.; Gill, P. M. W.; Johnson, B.; Chen, W.; Wong, M. W.; Gonzalez, C.; Pople, J. A. *Gaussian 03, revision D.01*; Gaussian, Inc.: Wallingford, CT, 2003.
- (21) Zeng, X. Q.; Gerken, M.; Beckers, H.; Willner, H. *Inorg. Chem.* **2010**, *49*, 3002–3010.
- (22) *CrysAlisPro, Version 1.171.33.42*, Oxford Diffraction Ltd.
- (23) Sheldrick, G. M. *SHELXL97*, University of Göttingen, 1997.
- (24) Mootz, D.; Merschenz-Quack, A. *Acta Crystallogr.* **1985**, *C41*, 924–925.
- (25) Besenyi, G.; Pákányi, L.; Foch, I.; Simándi, L. I.; Kálmán, A. *J. Chem. Soc., Perkin Trans. 2* **2000**, 1798–1802.